Vol. 591: 29–36, 2018
https://doi.org/10.3354/meps12414

MARINE ECOLOGY PROGRESS SERIES
Mar Ecol Prog Ser

Published March 19[§]

Contribution to the Theme Section 'Jellyfish bloom research: advances and challenges'

NOTE

Using unmanned aerial vehicles (UAVs) to measure jellyfish aggregations

Jessica Schaub[1,*], Brian P. V. Hunt[1,2,3], Evgeny A. Pakhomov[1,2,3], Keith Holmes[3], Yuhao Lu[4], Lucy Quayle[3]

[1]Department of Earth, Ocean and Atmospheric Sciences, University of British Columbia, Vancouver, British Columbia V6T 1Z4, Canada
[2]Institute of the Oceans and Fisheries, University of British Columbia, Vancouver, British Columbia V6T 1Z4, Canada
[3]Hakai Institute, PO Box 309, Heriot Bay, British Columbia V0P 1H0, Canada
[4]Integrated Remote Sensing Studio, Forest Sciences Center, 2424 Main Mall, Vancouver, British Columbia V6K 1Z4, Canada

ABSTRACT: Unmanned aerial vehicles (UAVs, or drones) are becoming increasingly common as tools to perform high-resolution but broad-scale measurements of habitats and populations simultaneously. In this study, we tested the application of UAVs to aerial surveys of jellyfish and their suitability for measuring and monitoring aggregations. We paired net hauls with linear image transects taken by a UAV to measure 5 *Aurelia* spp. aggregations over the course of 1 d in Pruth Bay, British Columbia, Canada. Georeferenced image transects were processed to determine aggregation areal extent and estimate percent cover of jellyfish. The percent cover estimates and net haul density data were highly comparable for all aggregations. Using combined UAV-derived surface area estimates and net haul biomass estimates, we calculated that jellyfish aggregation size ranged from 65 to 117 t wet weight biomass. We discuss the potential for additional UAV-based measurements including jellyfish abundance and individual size. The study demonstrates the potential of UAVs as powerful tools for characterizing and researching jellyfish aggregations *in situ*.

KEY WORDS: Drones · Jellyfish aggregations · GIS · Unmanned aerial vehicles

INTRODUCTION

Attention to jellyfish (broadly defined here as Scyphozoa and Hydrozoa) has increased in recent decades due to concern about the consequences of changing jellyfish populations in marine ecosystems (Purcell et al. 2007, Ruzicka et al. 2016). Jellyfish are known to form dense aggregations (Magome et al. 2007) and have a wide array of impacts on ecosystem processes, affecting predation and competition (Ruzicka et al. 2016), promoting carbon fluxes to the deep ocean (Lebrato et al. 2013, Sweetman & Chapman 2015), and changing the dissolved organic matter pool that fuels the microbial loop (Condon et al. 2011, Zeng et al. 2016). Despite the important ecological role of jellyfish aggregations, accurate estimates of their size, biomass, distribution, and movement are difficult to obtain using standard oceanographic net sampling due to the mismatch between small-volume discrete net samples relative to the large extent of aggregations (Fig. 1).

The near-surface orientation of jellyfish aggregations makes aerial surveys a potentially valuable tool for researching their horizontal extent and

*Corresponding author: jessica.schaub@alumni.ubc.ca
[§]Advance View was available online January 29, 2018

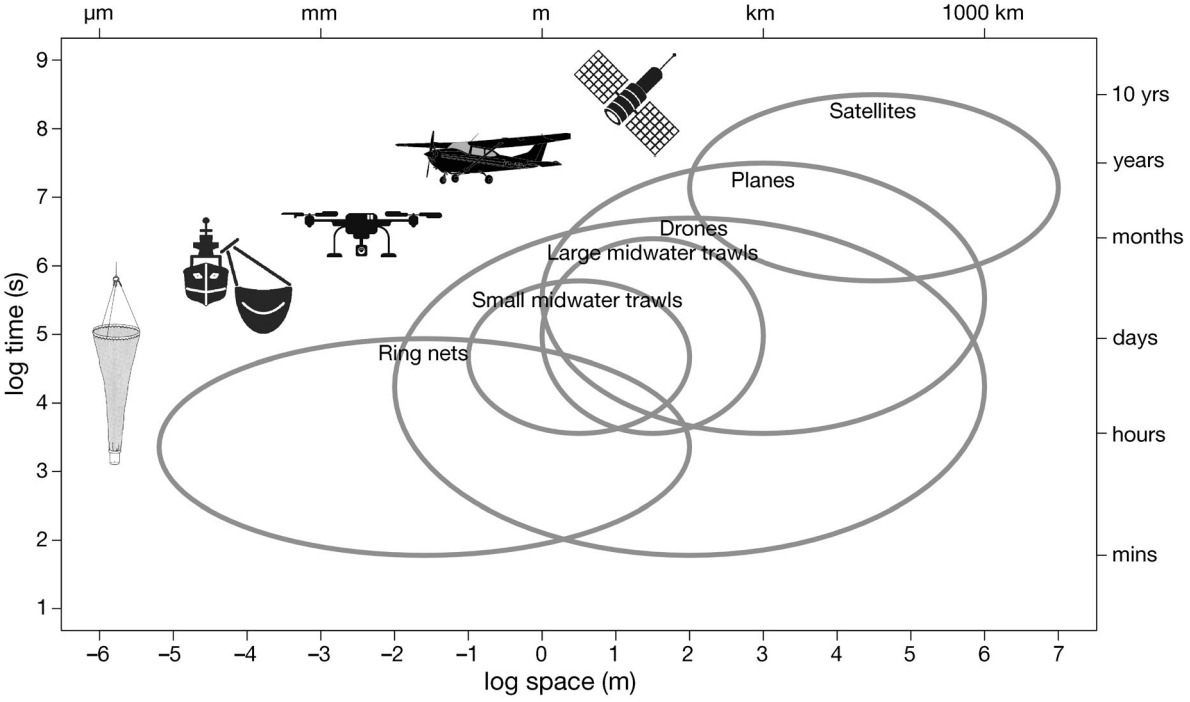

Fig. 1. Spatio-temporal scales of various oceanographic sampling techniques

temporal behaviour. To date, we are aware of 4 studies that have used manned aerial surveys via small aircraft to research jellyfish aggregations. Three of these studies used aerial photographs to locate and count aggregations (Purcell et al. 2000, Magome et al. 2007, Fossette et al. 2015), while one study used aerial surveys to estimate relative jellyfish species abundance (Houghton et al. 2006). These studies demonstrated the application of manned aerial surveys in researching the temporal and spatial aspects of jellyfish aggregations but also showed that the method has restricted spatial resolution and remains inaccessible to many researchers due to high costs.

Advances in unmanned aerial vehicle (UAV, or drone) technology have made aerial surveys a more accessible tool. UAVs are being increasingly used in terrestrial habitats where they can facilitate more accurate population surveys than ground counts, particularly in areas of challenging terrain (Hodgson et al. 2016). Although the use of UAVs in marine environments is relatively new, they have been used to monitor populations of large vertebrates including sharks, sea turtles, and dugongs (Hodgson et al. 2013, Bevan et al. 2015, Kiszka et al. 2016, Schofield et al. 2017). UAVs offer higher-resolution imagery and are more affordable than traditional aerial methods, while also offering non-disruptive alternatives to traditional monitoring techniques, such as net tows, tags, and manned aerial surveys (Hodgson et al. 2013, 2016, Bevan et al. 2015).

Based on the prior success of manned aerial surveys, we expect UAVs to enable accurate estimates of jellyfish aggregation parameters. In this study, we investigated the application of UAVs to (1) locate aggregations, (2) measure aggregation areal extent, (3) estimate relative jellyfish density, and (4) combine UAV with net-derived data to estimate total aggregation biomass. We highlight some of the pros and cons of using UAVs and point to key directions for further development of their application in jellyfish surveys.

MATERIALS AND METHODS

Sampling location and conditions

This study was conducted in Pruth Bay, in close proximity to the Hakai Institute field station on Calvert Island (British Columbia, Canada; Fig. 2, Supplement Video in Supplement 1 at www.int-res.com/articles/suppl/m591p029_supp/). Sampling was carried out on 11 September 2016 at 3 points in the tidal cycle: high tide in the morning, mid-ebb tide near midday, and low tide in the afternoon (Table 1). Environmental conditions were foggy during the first sampling period, affecting UAV image quality, but sunny to partly cloudy for the second and third sampling periods.

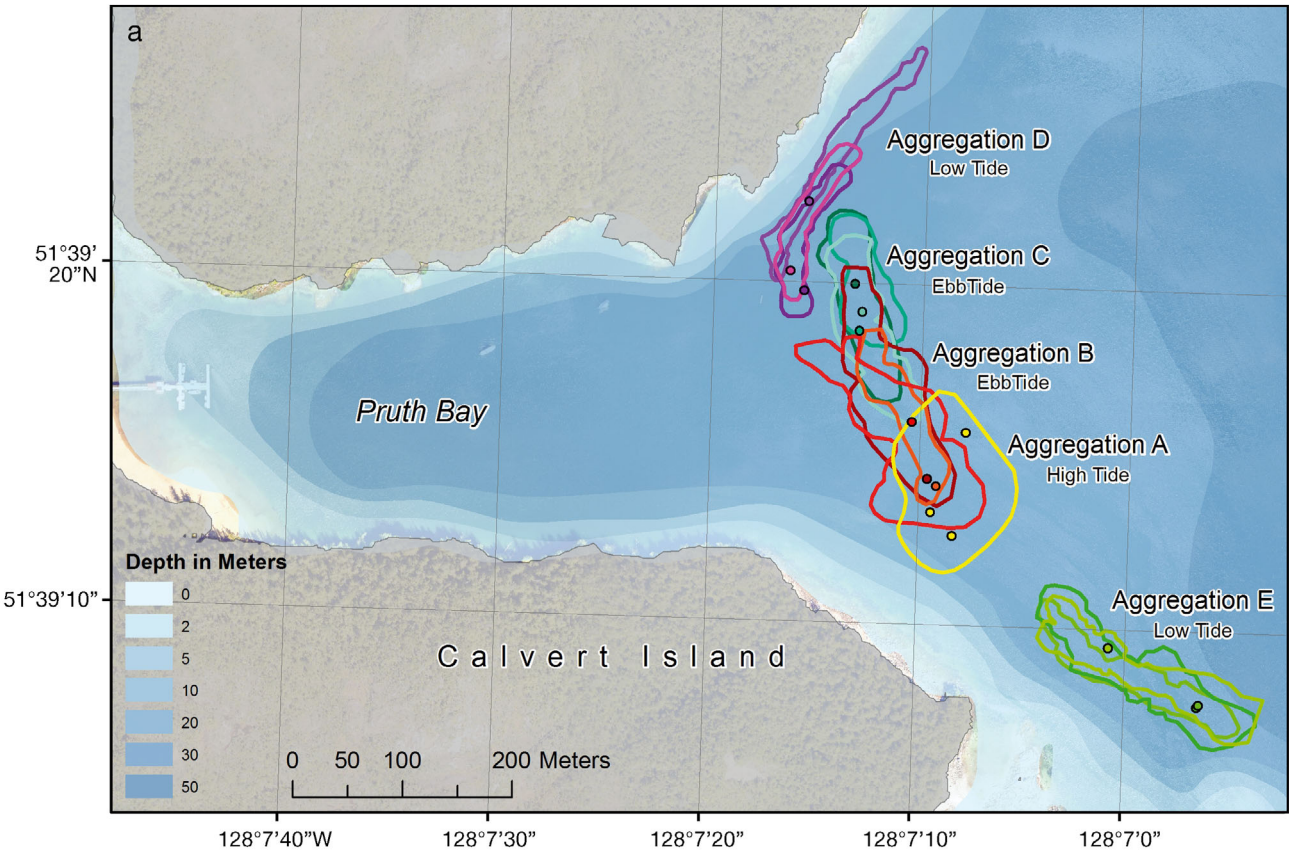

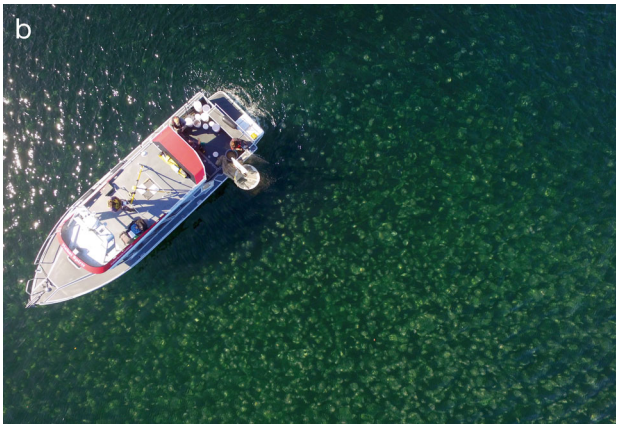

Fig. 2. (a) Sampling location and aggregate outlines. Aggregate outlines indicate the location of an aggregate at a particular tidal period. Different shades of the same colour class delineate the extent of the same bloom for each of the 3 image transects conducted at each tidal period. Points correspond to the coordinates of the net haul for the matching aggregate. The morning time period (yellow) had poor image quality due to foggy conditions, so only 1 outline could be made. (b) Unmanned aerial vehicle view of sampling vessel in *Aurelia* spp. aggregation

Field sampling

A DJI Phantom 3 Professional UAV equipped with a DJI 12 megapixel camera for capturing images at nadir (90° angle) was used for the aerial surveys. The use of track lines on the application map were used to plan imagery capture transects. The Phantom 3 UAV has a flight time of 15 to 18 min, and batteries were recharged on board the research vessel. At each sample time point, the following protocol was established: jellyfish aggregations were located with the UAV using the live feed from the DJI GO application (Fig. 2b). The sampling vessel was then positioned within the aggregation, and a vertical net haul was completed to a depth of 10 m using a 1 m diameter ring net. The net had 1000 µm mesh size and was equipped with a General Oceanics 2030r mechanical flow meter for volume filtered estimates. Three net samples were collected at different locations within each aggregation (Fig. 2a). Two aggregations were

Table 1. Details of sampling at each tidal period and the associated net and unmanned aerial vehicle (UAV)-based aggregation parameter estimates. Aggregation surface area was calculated from UAV data (see Fig. 2a)

Net haul	Time	Tide	Tidal peak time (h)	Aggregation	UAV transect	Flight altitude (m)	Pixel size obtained (m)	Smallest possible pixel size (m)	Aggregation surface area (m^2)	Net haul density (ind. m^{-3})	Net haul biomass (t m^{-2})	Total aggregation biomass (t)
1	09:26	High	09:55	A	D1[a]	50	0.058	0.022	12914[b]	0.314	0.001	85.3 ± 63.1
2	09:33				D2	60	0.099	0.026		2.099	0.011	
3	09:48				D3[a]	50	0.030	0.022		1.417	0.008	
4	11:39	Ebb	12:30	B	D4[a]	117	0.079	0.051	12531	2.439	0.012	83.1 ± 58.6
5	11:48				D5	120	0.081	0.052	4507	2.951	0.014	
6	11:58				D6[a]	120	0.078	0.052	10667	1.065	0.004	
7	12:17			C	D7	150	0.098	0.065	7067	3.455	0.014	117.4 ± 27.9
8	12:27				D8	150	0.167	0.065	4888	4.539	0.021	
9	12:43				D9[a]	150	0.123	0.065	6464	4.403	0.023	
10	15:08	Low	15:10	D	D10	100	0.071	0.043	3265	8.861	0.032	65.5 ± 39.3
11	15:19				D11	90	0.065	0.039	3167	5.400	0.020	
12	15:29				D12	100	0.065	0.043	4136	1.354	0.006	
13	15:56			E	D13	120	0.071	0.052	7671	1.462	0.008	106.1 ± 48.5
14	16:07				D14	120	0.065	0.052	9123	4.401	0.017	
15	16:17				D15	120	0.065	0.052	5567	3.655	0.018	

[a]Mapped with 2 transects instead of 1; [b]Due to fog, only 1 estimate of surface area for the 3 hauls was possible

measured at each time period, with the exception of the morning high tide when only 1 aggregation was located, resulting in 15 net hauls (Table 1).

While the vertical net hauls were taking place, a single linear transect was flown with the UAV along the long axis of the jellyfish aggregation. In a few instances, an aggregation required 2 image transects for complete mapping, which overlapped in some regions (Table 1). Transects ran from the sea towards shore using auto exposure to ensure the imagery was calibrated to maximize the visibility of the jellyfish. The flight altitude of the UAV varied from 50 to 150 m, depending on the transect (Table 1). Flight altitude was chosen based on weather conditions and desired image resolution, which determined the maximum altitude, and the size and complexity of the aggregation, which determined the minimum altitude. Transects were flown at 10 m s^{-1} or less to provide image clarity while limiting any effect of jellyfish drift. Manual imagery was captured every 1 s, aiming for >80% front image overlap, and included as much of the shoreline as possible to facilitate subsequent image stitching. Purposefully anchored small boats provided additional targets to facilitate stitching. Image pixel size varied from 30 to 160 mm, depending on the flight altitude (Table 1). Note that the software that was used for image processing decreased the image resolution during export, and it is in fact possible to achieve higher resolution (Table 1).

Sample processing

We did not differentiate between *Aurelia aurita* and *A. labiata* and present our data as *Aurelia* spp. Jellyfish with >50 mm bell diameter were enumerated and measured to the nearest 1 mm. This size class was exclusively *Aurelia* spp., with the exception of 1 *Cyanea capillata.* Overall, *Aurelia* spp. constituted approximately 99% of the jellyfish biomass in the net hauls. The *Aurelia* spp. diameter range was 70 to 360 mm with a mean of 230 mm (Fig. S1 in Supplement 2 at www.int-res.com/articles/suppl/m591p029_supp/). Count data were converted to densities using volume filtered data (jellyfish m^{-3}). Individual wet weight was measured for approximately 10% of the *Aurelia* spp. recovered in the net haul. The wet weights of the remaining individuals were estimated using a regionally specific length–weight relationship established by the Hakai Institute's Oceanography Program (Fig. S2 in Supplement 2):

$$\text{weight} = 0.00006 \times D^{2.9137} \quad (1)$$

where weight is the wet weight (g) and D is the bell diameter (mm). The individual wet weights were summed to estimate the biomass of each net haul in t m^{-2} (Table 1).

Image transects obtained by the UAV were mosaicked using Autostitch software, targeting 75% image overlap with ideally fewer than 20 images

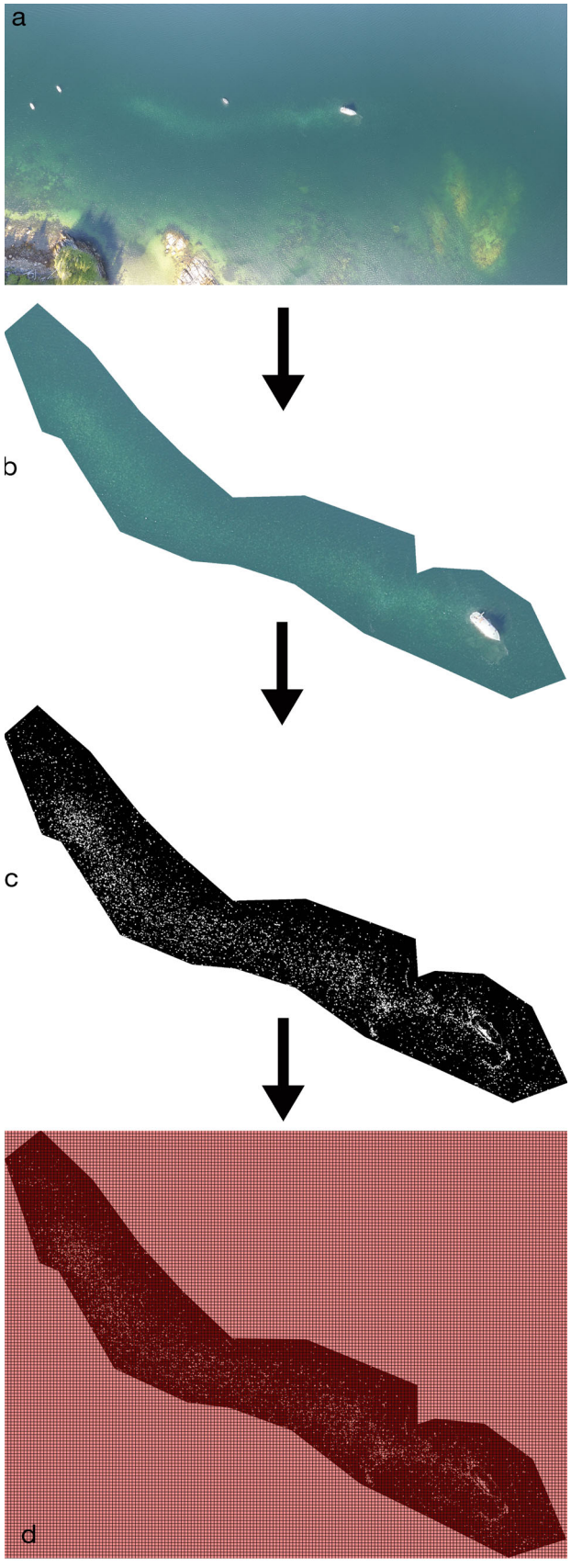

included in the finalized transect. Images were georeferenced and projected to BC Albers in ArcGIS 10.3.1 using land features, with a minimum of 10 targets for each image. A final spline transformation was applied to the images to account for the natural curvature of the landscape at the level of the coordinates (Fig. 3a). The combination of fog and the greater jellyfish depth during the morning period resulted in poor image results for the first aggregation, and we excluded this period from further analysis.

Post-georeference processing was carried out using QGIS 2.18.2 (QGIS Development Team 2009). The georeferenced files were stacked into a multi-layer raster image cube and analyzed using a texture analysis (ENVI 5.2) that took into account both the variance and data range of each of the 3 color bands (red [R], green [G], and blue [B]). The image stacks, comprising 9 bands (original, variance, and data range for each of R, G, and B), were cropped with a hand-drawn outline of the aggregation to avoid pixels with sun glare (Fig. 3b). Sun glare was an issue during this step, as it masked jellyfish presence. Where sun glare overlapped the border of the aggregation, the edge of the aggregation in the masked region was estimated by eye, introducing some subjectivity. A *k*-means clustering analysis was applied to group pixels according to differences and similarities in the 9 bands of the stacked image. Transect D5 (Table 1) had to be cropped into 2 small areas, one surrounding the boat and another in a different patch of the aggregation because of the high amount of glare.

Once clustered, the class that included the jellyfish was visually determined and extracted into a new image file (raster) which contained a single band of pixels that had values of either 1 (true, jellyfish) or 0 (false, not jellyfish) (Fig. 3c). A grid of 1 × 1 m square polygons was produced to overlay the raster to simulate 1 m^2 quadrats of the entire aggregation (Fig. 3d). An area of 1 m^2 was chosen to match the 1 m diameter of the sampling net, facilitating direct comparison of the net and image data. Zonal statistics of the true(1)/false(0) raster were calculated using the 1 m^2

Fig. 3. Jellyfish isolation and identification procedure. (a) Original stitched and georeferenced image (D15 in this case). (b) Stacked and cropped subset of the original image. Processing is carried out to isolate the area of interest and eliminate the effects of sun glare. (c) Resulting raster from the cluster analysis after extracting the class that contains jellyfish pixels (white). (d) Grid overlay of 1 m^2 quadrats for zonal statistics and calculating percent cover

quadrats as the defined zones, which resulted in a count and sum value for each quadrat. The count value for an individual 1 m^2 quadrat corresponded to the number of pixels it contained, and the sum corresponded to the number of those pixels that were jellyfish. These values were used to calculate the percent cover of jellyfish for each quadrat using the following equation:

$$\% \text{ cover} = \text{sum/count} \times 100\% \quad (2)$$

Since the cropped aggregations had irregular shapes and the grid of 1 m^2 quadrats that overlaid the image was rectangular (Fig. 3d), partial quadrats were produced on the aggregate margins. Quadrats were deemed to be completely overlaying the raster if the pixel count in that quadrat was >95% of the number of pixels that should be in a 1 m^2 quadrat (Table 1).

Finally, the calculated jellyfish aggregation area was multiplied by the mean jellyfish biomass (t m^{-2}) from the net hauls to estimate the total aggregation biomass (Table 1). This biomass calculation assumed that the depth of the aggregation was 10 m, matching the sampling depth of the vertical net hauls. However, footage from a camera attached to the mouth of the net showed that the depth of the aggregations exceeded 10 m, indicating that our biomasses are underestimates. We note too that the accuracy of the estimates would be enhanced by greater replication of vertical net hauls in each aggregate.

RESULTS AND DISCUSSION

The use of a UAV facilitated rapid and reliable location of jellyfish aggregations (Fig. 2), which is otherwise challenging from water level because of the limited horizontal view, and proved highly advantageous for positioning of the sampling vessel for net hauls. Previous studies have found that the use of UAVs in marine environments faces a specific subset of challenges, e.g. sun glare, turbidity, and wind strength during UAV deployment (Houghton et al. 2006, Hodgson et al. 2013, Bevan et al. 2015). Wind and turbidity were not a factor during our study but may be an issue seasonally and regionally. However, image quality was reduced under foggy conditions as well as in bright sun, when glare was a factor. Glare may be the greatest obstacle to the application of UAVs in aquatic surveys; however, there are a number of avenues for glare reduction. These include conducting UAV flights during overcast conditions, adjusting UAV flight paths to control the angle of the glare, and applying polarizing filters to the UAV camera lens. Reducing the glare in the original images could eliminate the need for cropping and allow automated identification of the aggregation extent.

Georeferencing the image transects enabled accurate calculation of the aggregation surface area, and this was a key element in the calculation of the total aggregation biomass. The high-resolution georeferenced imagery allowed for the detection of even small differences in the extent of the aggregations (e.g. within the same tidal period and through the day) (Fig. 2a), opening up the possibility for accurate high-frequency measurement and tracking of aggregation size, shape, and movement. This underscores a major advantage of using UAVs over manned aircraft for aerial surveys. The lower cost and ease of use of UAVs allow high-frequency repeated passes of a sampling area, enabling high temporal resolution monitoring and measurement of aggregations. Although our study was performed close to shore to facilitate stitching, it is possible to use photogrammetry software (e.g. Pix4D, Agisoft) to measure offshore aggregations. One of the few caveats with UAVs is a restricted operational range (in Canada this is 500 m, or 1000 m with additional Transport Canada certification) and regulations pertaining to operation near urban areas and airports. Local UAV regulations need to be assessed prior to UAV deployment.

Since UAV data provide a 2-dimensional value for the aggregation percent cover, and the net data produce a 3-dimensional estimate of density, the 2 data types are not directly comparable. Nevertheless, the percent cover estimates from the UAV imagery compared well with the estimates of net-derived density data when considering the relative differences between aggregations for each data type (Fig. 4), indicating a consistent trend between both data types. By combining the net haul and UAV data, we were able to estimate the total biomass of the aggregations (65 to 117 tons) (Table 1). As far as we know, these are the first estimates of total jellyfish aggregation biomass. Such estimates offer to improve calculations of jellyfish predation impact and carbon cycling.

UAV detection and mapping of jellyfish aggregation areal extent, in combination with net-derived density and/or biomass estimates, provide a novel approach to improved jellyfish biomass estimates that cannot easily be achieved by boat sampling alone. Although precise jellyfish aggregation biomass estimates require *in situ* net data on the vertical extent of the aggregation and its mean density, coarse estimates of jellyfish aggregation biomass

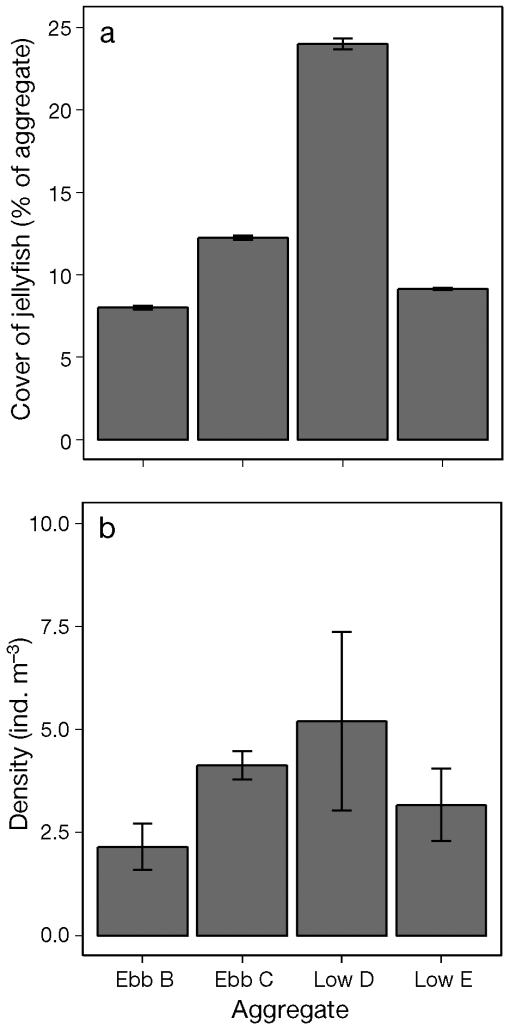

Fig. 4. (a) Unmanned aerial vehicle data. Mean percent cover of jellyfish in 1 m^2 quadrats overlaying image transects of the aggregations (*x*-axis, tide condition indicated). (b) Net data. Mean density of jellyfish from 10 m vertical net hauls. Each aggregation had at least 3 image transects and 3 vertical net hauls that were processed individually (see Table 1). Error bars represent SE

could be calculated using aerial survey data alone, if estimates of individual jellyfish bell diameter can be obtained from the imagery. An important parameter in size estimates is the pixel size of the images. Pixel size varies with flight altitude (Table 1) and can be modified to accommodate a range of species diameters. Once the size of individuals has been determined, a length–weight relationship can be applied to produce biomass estimates. A final element of this process will be a database of direct comparisons between net data and UAV data, to determine the level of disparity between the true density (net haul) and the estimated density (image results) and correct for the disparity. Reaching semi-quantitative estimates of aggregation biomass would extend the value of UAVs for routine observation beyond simply mapping the areal extent and relative density (percent cover) of aggregations.

This pilot study demonstrated that UAVs can be used to make both qualitative and quantitative measurements of jellyfish aggregations and provide solutions to the challenges faced by jellyfish monitoring using vessel sampling. Georeferenced images made it possible to accurately calculate aggregation location and extent, and high-resolution imagery allowed for measurements on a finer scale than previously obtained by traditional aerial methods. Because of the cost effectiveness of data acquisition and processing (made possible through open-source software packages), UAVs present a realistic option for high temporal and spatial resolution monitoring and research of jellyfish aggregations.

Acknowledgements. This research was funded by the Tula Foundation. We thank the staff of Hakai Institute for assistance in all phases of this research. Bryn Fedje, Nelson Roberts, and Emma Myers assisted in field data collection.

LITERATURE CITED

Bevan E, Wibbels T, Najera BM, Martinez MA and others (2015) Unmanned aerial vehicles (UAVs) for monitoring sea turtles in near-shore waters. Mar Turtle Newsl 145: 19–22

Condon RH, Steinberg DK, del Giorgio PA, Bouvier TC, Bronk DA, Graham WM, Ducklow HW (2011) Jellyfish blooms result in a major microbial respiratory sink of carbon in marine systems. Proc Natl Acad Sci USA 108: 10225–10230

Fossette S, Gleiss AC, Chalumeau J, Bastian T and others (2015) Current-oriented swimming by jellyfish and its role in bloom maintenance. Curr Biol 25:342–347

Hodgson A, Kelly N, Peel D (2013) Unmanned aerial vehicles (UAVs) for surveying marine fauna: a dugong case study. PLOS ONE 8:e79556

Hodgson JC, Baylis SM, Mott R, Herrod A, Clarke RH (2016) Precision wildlife monitoring using unmanned aerial vehicles. Sci Rep 6:22574

Houghton JDR, Doyle TK, Davenport J, Hays GC (2006) Developing a simple, rapid method for identifying and monitoring jellyfish aggregations from the air. Mar Ecol Prog Ser 314:159–170

Kiszka JJ, Mourier J, Gastrich K, Heithaus MR (2016) Using unmanned aerial vehicles (UAVs) to investigate shark and ray densities in a shallow coral lagoon. Mar Ecol Prog Ser 560:237–242

Lebrato M, Mendes PJ, Steinberg DK, Cartes JE and others (2013) Jelly biomass sinking speed reveals a fast carbon export mechanism. Limnol Oceanogr 58:1113–1122

Magome S, Yamashita T, Kohama T, Kaneda A, Hayami Y, Takahashi S, Takeoka H (2007) Jellyfish patch formation investigated by aerial photography and drifter experi-

ment. J Oceanogr 63:761–773
Purcell JE, Brown ED, Stokesbury KDE, Haldorson LH, Shirley TC (2000) Aggregations of the jellyfish *Aurelia labiata*: abundance, distribution, association with age-0 walleye pollock, and behaviors promoting aggregation in Prince William Sound, Alaska, USA. Mar Ecol Prog Ser 195:145–158
Purcell JE, Uye SI, Lo WT (2007) Anthropogenic causes of jellyfish blooms and their direct consequences for humans: a review. Mar Ecol Prog Ser 350:153–174
QGIS Development Team (2009) Geographic information system. Open Source Geospatial Foundation. http://qgis.osgeo.org
Ruzicka JJ, Daly EA, Brodeur RD (2016) Evidence that summer jellyfish blooms impact Pacific Northwest salmon production. Ecosphere 7:e01324
Schofield G, Papafitsoros K, Haughey R, Katselidis K (2017) Aerial and underwater surveys reveal temporal variation in cleaning-station use by sea turtles at a temperate breeding area. Mar Ecol Prog Ser 575:153–164
Sweetman AK, Chapman A (2015) First assessment of flux rates of jellyfish carcasses (jelly-falls) to the benthos reveals the importance of gelatinous material for biological C-cycling in jellyfish-dominated ecosystems. Front Mar Sci 2:47
Zeng Y, Huang X, Huang B, Mi T (2016) Relationship between bacteria and phytoplankton during the giant jellyfish *Nemopilema nomurai* bloom in an oligotrophic temperate marine ecosystem. Acta Oceanol Sin 35: 107–113

Editorial responsibility: Robert Condon, Wilmington, North Carolina, USA

Submitted: June 7, 2017; Accepted: November 9, 2017
Proofs received from author(s): December 29, 2017